



Nanoindentation behaviors of amorphous carbon films containing nanocrystalline graphite and diamond clusters prepared by radio frequency sputtering

Xue Fan^{a,b}, Kenji Nose^c, Dongfeng Diao^{a,d,*}, Toyonobu Yoshida^b

^a Key Laboratory of Education Ministry for Modern Design and Rotor-Bearing System, School of Mechanical Engineering, Xi'an Jiaotong University, Xi'an 710049, China

^b Department of Materials Engineering, Graduate School of Engineering, The University of Tokyo, Tokyo 113-8656, Japan

^c Institute of Industrial Science, The University of Tokyo, Tokyo 153-8505, Japan

^d Nanosurface Science and Engineering Research Institute, Shenzhen University, Shenzhen 518060, China

ARTICLE INFO

Article history:

Received 9 September 2012

Received in revised form 29 January 2013

Accepted 4 March 2013

Available online 14 March 2013

Keywords:

Nanocrystalline
Carbon film
Amorphous
Graphite
Diamond
Nanoindentation

ABSTRACT

Amorphous carbon (a-C) films were prepared by a radio-frequency sputtering method. Nano structures in the films were controlled by changing the ion irradiation energy and deposition temperature. It was found that nanocrystalline graphite and diamond clusters were embedded in the pure amorphous structure with sizes of approximately 5 nm. a-C films contained nanocrystalline graphite clusters (a-C:NCG) were obtained with the ion energy ranging from 50 to 120 eV and temperature in 300–370 K. a-C film contained nanocrystalline diamond clusters (a-C:NCD) was obtained with 120 eV at 570 K. Nanoindentation behaviors of these carbon films were compared with pure amorphous structured carbon film. The percentage of elastic recoveries of a-C:NCD, a-C, and a-C:NCG films were obtained to be 81.9%, 84.3%, and 87.5%, respectively. Pop-in steps with about 3 nm displacement appeared in loading curves for a-C:NCG film, and 10 nm for a-C:NCD film. These results showed that the nanoindentation behaviors of amorphous carbon film containing cross-linked nanocrystalline graphite clusters is better than that of diamond clusters.

© 2013 Elsevier B.V. All rights reserved.

1. Introduction

Nanocrystalline carbon structures include for example graphite, diamond, fullerene, nanotube, and graphene, and these structures contribute to their unique characteristics [1]. When nanocrystalline structured clusters are embedded in the amorphous carbon (a-C) matrix, the excellent characteristics of these clusters enhance the overall properties of the films. Therefore, the study of a-C films including nanocrystalline clusters has attracted much attention. It has been reported that a-C films containing graphite and fullerene clusters exhibited good mechanical properties with higher hardness and elastic recovery [2,3] and unique electrical properties [4,5] without compromising the tribological properties [6]. When carbon nanotubes were embedded into a-C, the field emission current was significantly increased [7]. Lately, graphene sheet embedded carbon films with the π -electronic structure of bilayer graphene have been prepared by low-energy electron irradiation, and the films can

be expected to be applicable in many areas in electronics [8]. The formation of nanocrystalline structure mainly depends on the film preparation technology.

Different methods have been tried to make nanocrystalline structures in a-C films, for example the filtered cathodic arc deposition [9], energetic particle bombardment [10], pulsed laser deposition [11,12], and radio-frequency (RF) sputtering [13,14]. In RF sputtering, ion energy from plasma varies in a wide range, and is easy to control to promote and modify the growth of nanocrystalline structures in BN films [15]. Schwan et al. observed carbon films deposited by RF sputtering and found that small graphite regions appeared although the film had a high sp^3 content [13]. Wan and Komvopoulos used a magnetron sputtering system to prepare a-C films and observed clusters of nanocrystalline diamond in these films. They suggested that through the irradiation of argon ions, the sp^2 bonds in the a-C films were broken and rebound to form diamond clusters [16,17]. Lau et al. studied the ion energy and substrate temperature effects on the nanostructure of carbon films prepared by filtered cathodic arc deposition, and showed that relatively high temperature (713 K) and moderate ion energy (95 eV) were proper conditions to form sp^2 -bonded nanocrystalline clusters [18]. However, in the RF sputtering system, less is known about

* Corresponding author at: Nanosurface Science and Engineering Research Institute, Shenzhen University, Shenzhen 518060, China. Tel.: +86 755 26902415.

E-mail address: dfdiao@szu.edu.cn (D. Diao).

Table 1
Deposition conditions of the investigated samples.

Sample	A	B	C	D	E
Substrate bias, s.Vdc (V)	−30	−60	−100	−100	−100
Ion energy (eV) ^a	50	80	120	120	120
Substrate temperature, T _S (K)	300	300	300	370	570
Thickness (nm)	75	70	60	62	67

^aCalculated by (−s.Vdc + 20) eV.

the effects of ion energy and deposition temperature on controlling the formation of nanocrystalline clusters in a-C films.

When carbon films are applied as protective coatings, excellent mechanical properties to sustain internal stress and resist delamination are needed. As mentioned above, the properties of carbon films are potentially improved with the inclusion of nanocrystalline clusters. It has been revealed that graphite clusters embedded in an amorphous matrix show good mechanical properties. When the *sp*²-bonded nanocrystalline structure was embedded in the amorphous matrix, the *sp*²-bonded structure enhanced the flexibility and elastic recovery, as determined by nanoindentation [19–21], and the hardness can be increased with *sp*³ bonds connecting the *sp*²-bonded sheets [22]. However, much less is studied about the indentation behaviors of a-C films containing nanocrystalline diamond clusters.

When we characterize the mechanical properties of materials with nanocrystalline structures inside of them, both the external geometry and the internal local structure should be considered [23]. This is because the generation and progress of plastic deformation are both related to the actual indentation size, and they affect the overall fracture behaviors of the films [24]. However, for the a-C films containing nanocrystalline structures, people usually focused on their excellent overall elastic and hardness constants. Consequently, the detailed nanoindentation behavior of a-C films with nanocrystalline clusters is an open question, and it is interesting to know if there is difference between the nanoindentation behaviors of the carbon films containing nanocrystalline graphite and diamond clusters.

Therefore, in this study, the controlling effects of ion irradiation energy and deposition temperature on the nanostructures of carbon films in radio-frequency (RF) sputtering are revealed. Then, the nanoindentation behaviors of a-C films with nanocrystalline graphite and diamond clusters are examined.

2. Experiments

2.1. Film preparation

An RF (13.56 Hz) sputtering system [25] was used to deposit carbon films on monocrystalline silicon (100) substrates of 20 mm × 20 mm × 0.5 mm. The chamber was pumped to a high vacuum (base pressure < 2.6 × 10^{−5} Pa) with a turbomolecular pump. Pure argon was employed as the working gas with a pressure of 1.33 Pa. A graphite carbon plate was used as the target, and Si substrates were placed 50 mm away facing the target. Before film deposition, the native oxide of the substrate surface was removed with a −100 V substrate negative direct-current bias in RF (s.Vdc) for 15 min. The mean ion energy was estimated to be approximately (−s.Vdc + 20) eV [26], therefore, the substrate was physically etched with an argon ion energy of 120 eV. The RF power applied to the graphite target was maintained at 150 W during deposition. Ion energy and deposition temperature are the two factors that control the nanostructures in the carbon films, and they were adjusted by s.Vdc and the substrate temperature (T_S), respectively. Table 1 shows the deposition conditions of Sample A–E investigated in this

study. All the films were deposited for 25 min at the deposition rate of 2.4–3 nm/min.

2.2. Characterizations

The nanostructures of carbon films were observed by transmission electron microscopy (TEM, JEOL-2010) operated with the electron acceleration voltage of 300 kV (the two-point resolution was 0.17 nm). TEM specimens for the cross-sectional view were prepared by mechanical polishing followed by argon-ion beam milling to a thickness appropriate for observation, and those for plan view observation were prepared by scratching the film with a diamond stylus, and then transferring the films onto a copper microgrid. The chemical bonding structures of *sp*² and *sp*³ hybridized carbon atoms were analyzed by X-ray photoelectron spectroscopy (XPS) with monochromatic Al K α radiation (150 W, 15 kV). The film surfaces were cleaned by argon ions before analysis, and then scanned from 0 to 1200 eV of binding energy. The nanocrystalline clusters in the samples were studied from Raman spectra, which were obtained using a Raman spectrometer (JASCO NRS-5100) with a laser wavelength of 532 nm. The power of the laser beam was set to 5.5 mW to minimize the laser-induced damage to the sample, and the beam was focused to 1 μ m². In this study, the spectra between 1100 and 1800 cm^{−1} were acquired, and the spectral resolution was 0.4–1 cm^{−1}. Surface topologies of the carbon films were measured by atomic force microscopy (AFM, SHIMAZU SPM-9700) with a scan size of 0.5 μ m × 0.5 μ m. Nanoindentation behaviors were tested using a Hystron nanoindenter with a Berkovich tip. The tip has a total included angle of 142.2° with tip radius between 100 nm and 200 nm. The elastic modulus of 72 GPa for a quartz silica was selected for contact area calibration. The loads of 500, 800, and 2000 μ N were chosen to study the nanoindentation behaviors, and all of the load displacement curves were confirmed by two or three indentation tests under same conditions.

3. Results

3.1. Nanostructures

Fig. 1 shows TEM images and diffraction patterns of the carbon films. The nanostructure of Sample A is purely amorphous, as shown in the plan view image and the diffraction pattern (Fig. 1(a)). The a-C film was prepared at a low temperature of 300 K (room temperature) and low ion energy of 50 eV. When the temperature was kept at 300 K, while increasing the ion energy to 80 and 120 eV, nanocrystalline clusters with a layer space of 0.34 nm appeared in the films, as seen in Figs. 1(b) and (c). The layer space value matches the (002) spacing of bulk graphite. These clusters of nanocrystalline graphite (NCG) were randomly distributed and oriented in the amorphous matrix. The basal planes of NCG were cross-linked with each other by waving and twisting, as shown in the enlarged blocks in Fig. 1(b) and (c). The electron diffraction patterns show clearer rings compared with that of the purely amorphous structure, which also supports the generation of a nanocrystalline structure in the amorphous matrix. Fig. 1(c-2) shows the representative cross-sectional view of the carbon film with NCG clusters (Sample C). The same nanocrystalline sheets with layer space of 0.34 nm can also be found in the enlarged view. When the ion energy was 120 eV, and the temperature was increased to 370 K, the film structure did not change compared with that of the film deposited at a temperature of 300 K, as shown in Fig. 1(d). Samples B–D were all a-C films containing nanocrystalline graphite clusters (a-C:NCG). However, when the temperature was increased to 570 K, Fig. 1(e) shows that in addition to the graphite clusters,

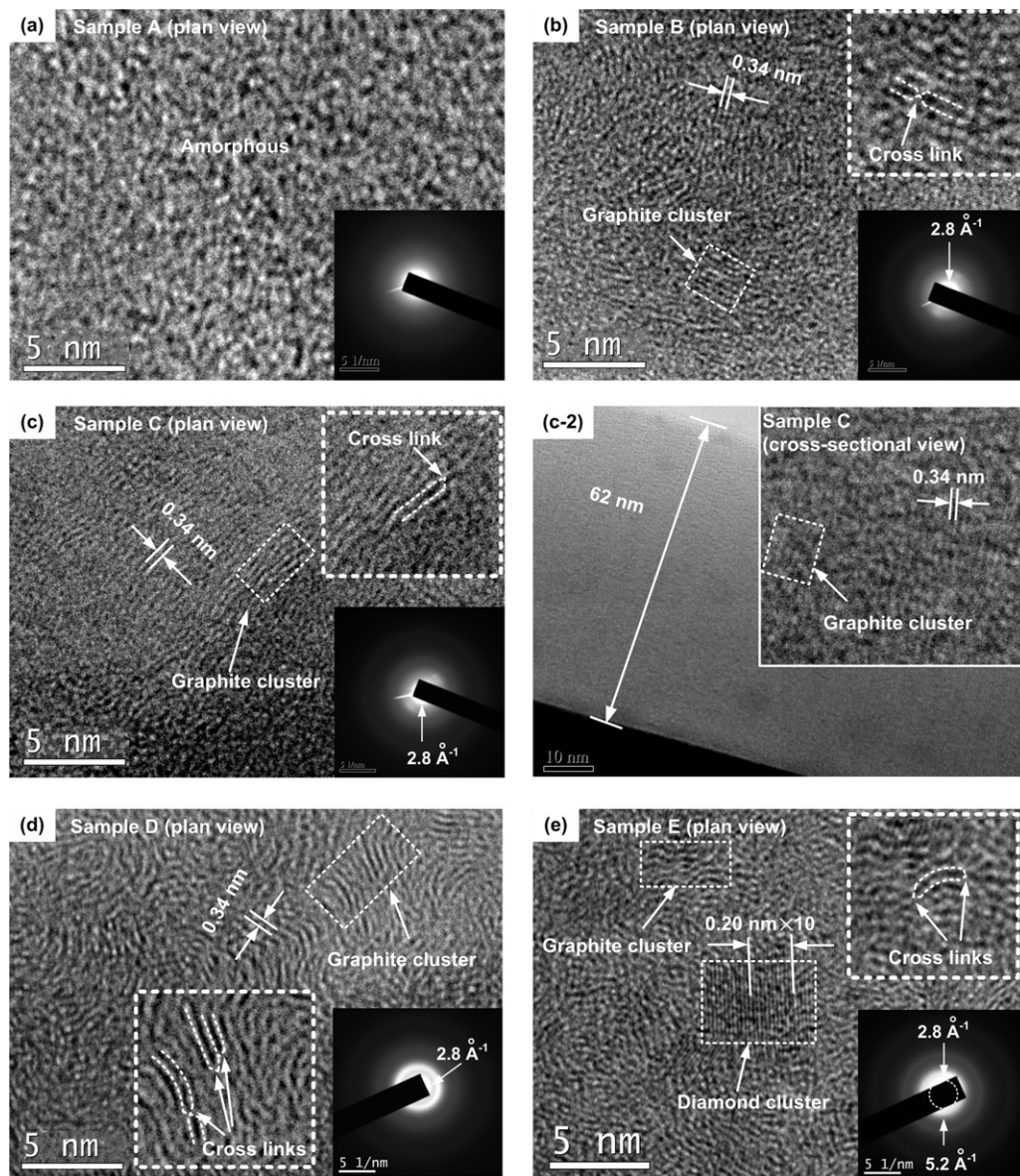


Fig. 1. Nanostructures of carbon films observed by TEM.

straight planes with a constant distance of about 0.2 nm were presented. This structure is inferred to be nanocrystalline diamond (NCD) [4,27]. The cluster size of NCDs was about 5 nm, and the distribution and orientation were random in the amorphous matrix as in the case of NCG. Therefore, from the TEM observations, the structure of the prepared carbon films was modified from pure a-C to a-C:NCD when the ion energy was increased from 50 to 120 eV. Then, when the ion energy was held at 120 eV and the deposition temperature was increased to 570 K, the structure changed to a-C containing both NCG and NCD clusters (a-C:NCD for short).

Chemical bonds in the films, i.e., sp^2 and sp^3 hybridized carbon atoms, were characterized by XPS. Fig. 2 shows the typical spectrum of C 1s of the carbon film. In order to quantitatively obtain the sp^2 and sp^3 contents in the investigated carbon films, the original C 1s spectrum was deconvoluted into three Gaussian distribution curves. The two curves with peak positions at binding energies of 284.4 and 285.2 eV represented the sp^2 and sp^3 hybridizations, respectively. Another weak curve with a peak position at 288.8 eV indicated C–O bonds, which meant that a small amount of oxygen was included in the film. The ratio of sp^3 to sp^2 contents is shown in

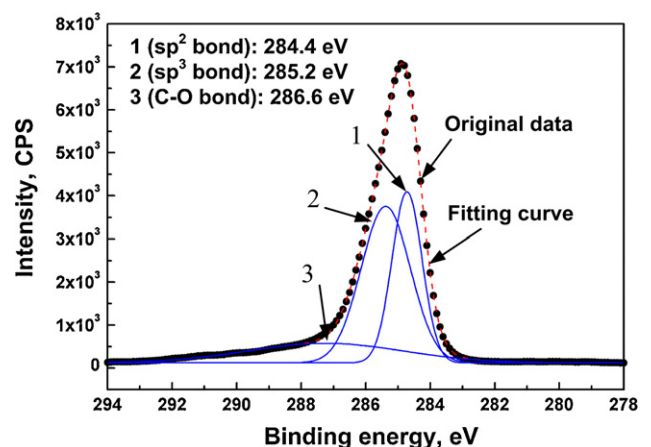


Fig. 2. C 1s core level spectrum and fitting curves of carbon film (Sample C).

Table 2
G peak position shift and peak intensity ratio of D peak to G peak.

Carbon films	a-C	a-C:NCG			a-C:NCD
	Sample A	Sample B	Sample C	Sample D	Sample E
sp^3/sp^2	1.72	1.49	1.47	1.24	1.61
G peak position (cm^{-1})	1571.6	1569.6	1570.8	1578.8	1591.4
I_D/I_G	0.368	0.269	0.299	0.477	0.677

Table 2. The content of sp^3 hybridization was higher than that of sp^2 hybridization in all of the investigated samples because the incident ion energy during the deposition provides pressure to form the sp^3 hybridization. Sample A with the purely amorphous structure had the highest sp^3 content. Then, with the increase in ion energy to 120 eV and temperature to 370 K, the sp^3 content decreased gradually. It was also verified from the TEM images which showed the existence of NCG clusters in Samples B–D. On the other hand, in Sample E, since the NCD clusters were embedded, the sp^3 content increased again.

The clustering process of NCG is associated with a change in the Raman spectrum [28]. Fig. 3 shows the Raman spectra of the investigated carbon films. Sample A (a-C) shows a relatively wide band, Samples B–D (a-C:NCG) exhibit a clearer G peak in the Raman spectra, and for Sample E (a-C:NCD), the D peak and G peak were separated. Since the G peak involves the in-plane bond (chains or rings) of sp^2 carbon atoms, and the D peak indicates the organization of sp^2 carbon atoms into nanoclusters of sp^2 -bonded sixfold rings, the change in the Raman spectra was in accordance with the structural transformations of sp^2 clusters in the films [29].

To examine the structural transformation in detail, the Raman spectra in Fig. 3 were deconvoluted to D and G peaks. The G peak was fitted with a Breit–Wigner–Fano (BWF) function and the D peak with a Lorentzian one [29]. The G peak position and the intensity ratio of the D peak to the G peak (I_D/I_G) are listed in Table 2. Increasing the ion energy from 50 to 120 eV at 300 K, the G peak position barely changed with the variation of ion irradiation energy, however, it goes to higher values when increasing the temperature. An upward shift in the G peak position signifies sp^2 carbon aggregation into larger clusters with shorter nearest-neighbor distances [30]. Sample E also showed an increasing G peak position, which indicated that sp^2 bonds can condense into larger clusters at higher temperature even with increased sp^3 content. This is because the sp^2 bond is able to diffuse in the a-C matrix and the activation energy of the diffusion is lower than the conversion energy of sp^3 to sp^2 [31]. The peak density ratio of I_D/I_G was used to monitor the

evolution of graphitization in the films since I_D/I_G is normally proportional to the clustering of rings. The results of I_D/I_G showed the same trend for the G peak position as mentioned above. The higher the I_D/I_G , the more clusters of NCG with sp^2 bonds are embedded in the amorphous matrix.

3.2. Surface topographies

Surface topographies of the investigated carbon films and Si substrate are shown in Fig. 4. The mean surface roughnesses (R_a) of Samples A (0.052 nm), B (0.050 nm), and C (0.065 nm) were all smaller than that of Si substrate (0.081 nm). The sputtered ion energy barely changed the surface roughness at room temperature even if the nanostructure of the films was modified from a-C (Sample A) to a-C:NCG (Samples B and C). When increasing the temperature from 300 to 370 K, R_a of Sample D (0.62 nm) increased about tenfold compared with that of Sample C, as shown in Fig. 4(d), and there were small domes on the surface. Then, upon increasing the substrate temperature to 570 K, R_a reached 2.74 nm for Sample E and large domes appeared on the film surface dispersedly.

3.3. Nanoindentation behaviors

Nanoindentation behaviors of the carbon films were analyzed from load–displacement curves. Fig. 5 shows the typical load–displacement curves of three different nanostructured carbon films and the Si substrate with the maximum indentation load of 500 μN . All the curves showed consecutive loading and unloading processes. On the basis of the load–displacement curves, the hardness (H) and elastic modulus (E) are usually evaluated by the approach proposed by Oliver and Pharr [32]. The maximum indentation depth (h_{max}), the residual indentation depth (h_{res}), and the elastic recovery (R) are also calculated in relation to H and E . The maximum indentation depth (h_{max}) indicates the stiffness of the film. Elastic recovery (R) is a factor that affects the ability to prevent plastic deformation, and the percentage of R (% R) is calculated using h_{res} and h_{max} , as expressed in the following [33]:

$$\%R = \frac{(h_{\text{max}} - h_{\text{res}})}{h_{\text{max}}} \quad (1)$$

The values of h_{max} and % R for Samples A–E with indentation load of 500 μN are listed in Table 3. For comparison, the values of hardness and elastic modulus calculated by the Power Law Relation with calibrated contact area function were given in the table. Compared with the Si substrate, the a-C film showed a much smaller h_{max} under the same indentation load. Upon increasing ion energy and deposition temperature, the maximum indentation depths of a-C:NCG films slightly increased compared with the a-C film, indicating that the a-C:NCG films became slightly softer, but were still harder than the substrate, which can be reflected from the hardness value. When clusters of NCD were embedded in the amorphous matrix (Sample E), the values of h_{max} and calculated hardness were near that of the substrate. That is, the hardness decreased considerably for the a-C:NCD film. As mentioned above, % R is related to the elastic properties of the material. The Si substrate had the % R value of only 71.4%, and for the carbon film with purely amorphous structure, % R was approximately 84.3%. When clusters of NCG were

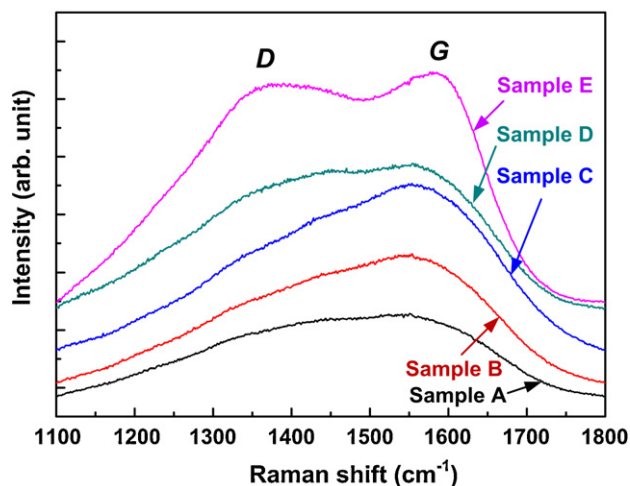


Fig. 3. Raman spectra of carbon films.

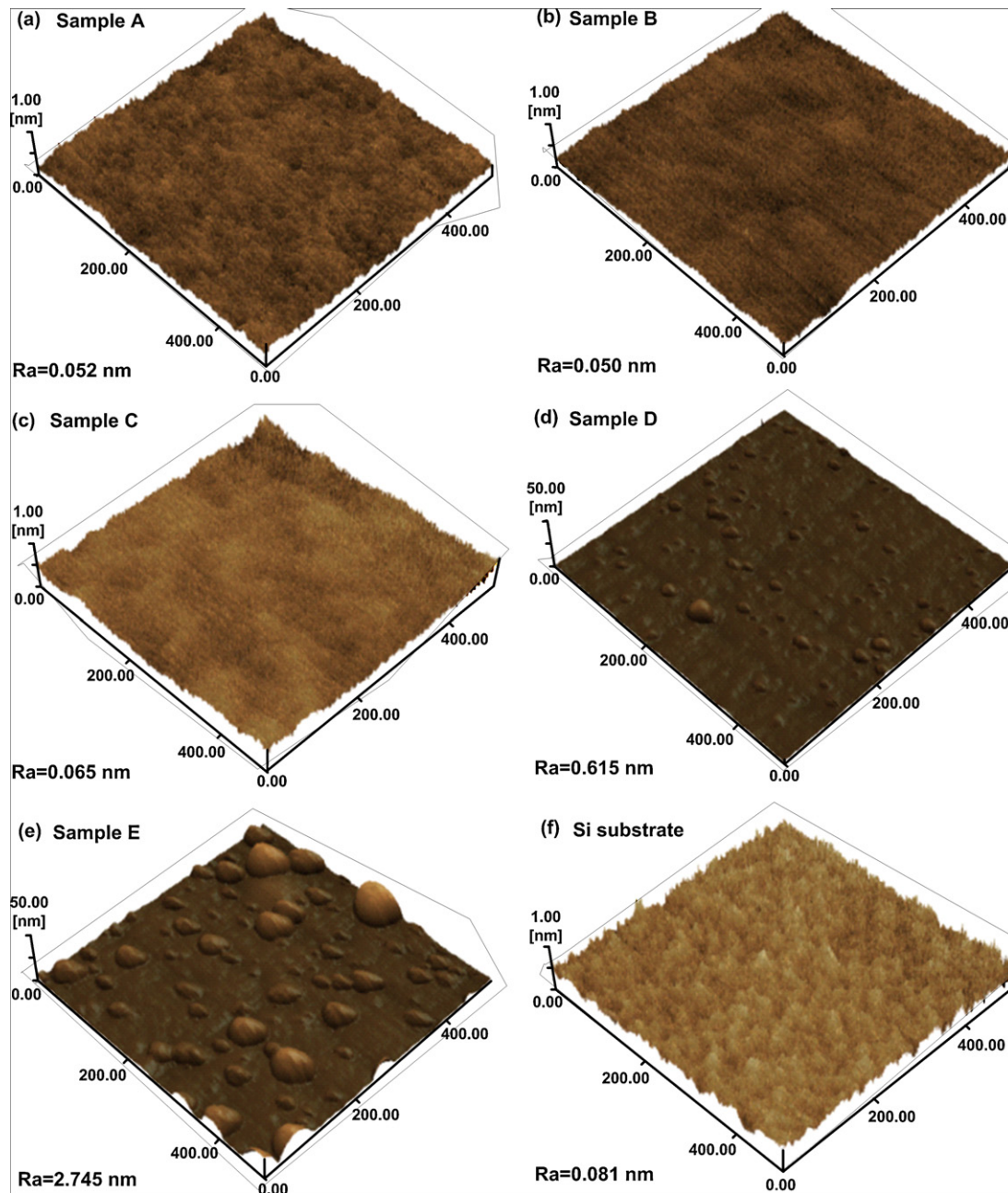


Fig. 4. Surface topographies of carbon films from (a) to (e) for Samples A–E respectively, and that of Si substrate (f).

embedded, %R was increased to 87.5%. However, %R decreased to 81.9% when NCD clusters were embedded. Although the sp^3 content increased comparing with a-C:NCG, the hardness and elastic recovery of a-C:NCD film were both decreased.

Depending on the types of clusters embedded into a-C, the load–displacement curves showed different characteristics more prominently when the maximum indentation load was increased

(i.e., the indentation area was enlarged). The load–displacement curves of the Si substrate and a-C film exhibited continuous loading and unloading curves under indentation load of 800 μN , as shown in Fig. 6. However, for a-C:NCG and a-C:NCD, the loading curves showed small but clear discontinuous pop-in steps of about 3 nm displacement, as indicated in Fig. 6(a) and the enlarged view in Fig. 6(b). Continuously increasing maximum indentation load to

Table 3

Maximum indentation depth, hardness, elastic recovery, and elastic modulus for the investigated samples obtained with nanoindentation load of 500 μN .

Sample	Si Substrate	a-C Sample A	a-C:NCG			a-C:NCD Sample E
			Sample B	Sample C	Sample D	
Maximum indentation depth, h_{max} (nm)	42.0	35.0	35.9	36.6	37.1	41.4
Hardness, H (GPa)	11.01	19.12	18.04	16.01	15.28	12.27
% Elastic recovery, %R	71.4%	84.3%	87.5%	86.3%	85.2%	81.9%
Elastic modulus, E (GPa)	151.08	170.74	170.47	172.12	154.80	148.56

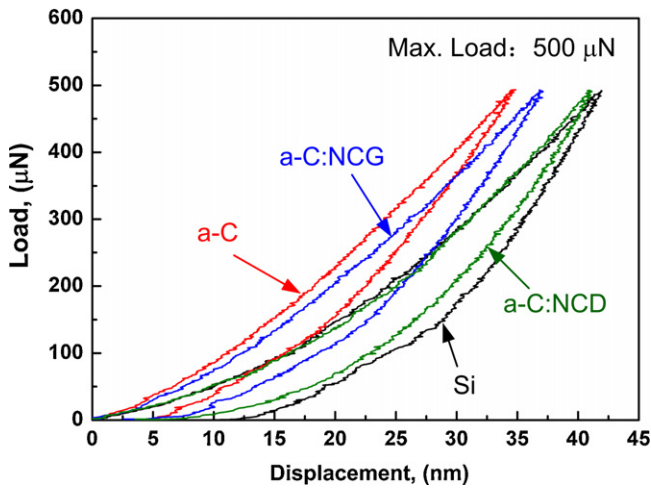


Fig. 5. Load–displacement curves with maximum indentation load of 500 μN .

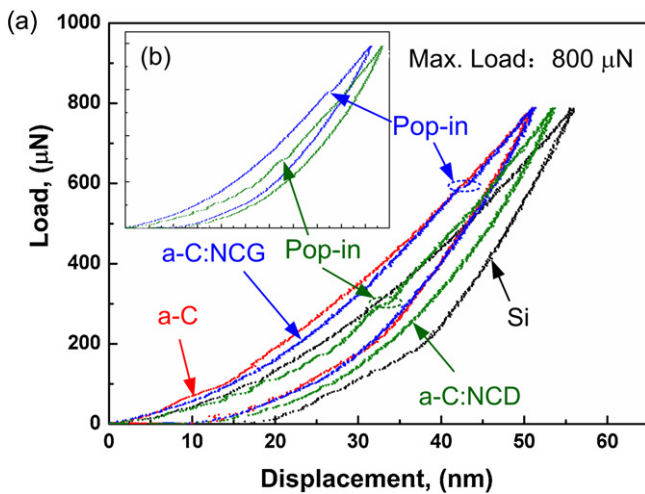


Fig. 6. Load–displacement curves with maximum indentation load of 800 μN .

2000 μN , the load–displacement curves were shown in Fig. 7. The loading and unloading curves showed continuity for the Si substrate and a-C film. Small discontinuous pop-in steps existed in the loading curve of a-C:NCG film. However, when the indentation load on a-C:NCD film reached the maximum, a large step of about 10 nm

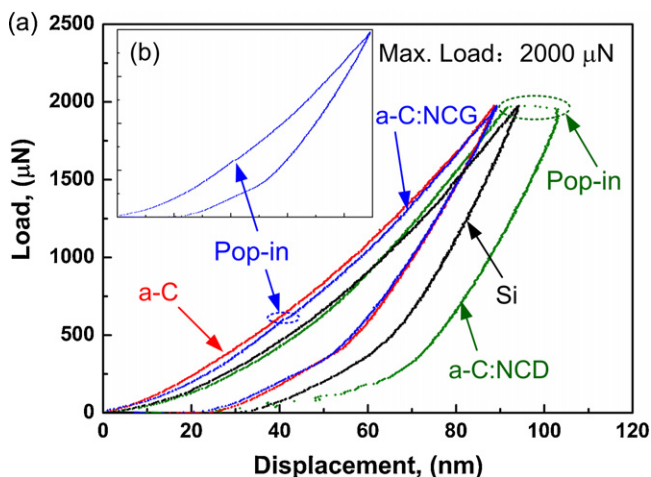


Fig. 7. Load–displacement curves with maximum indentation load of 2000 μN .

starting from the displacement of 90 nm can be observed. Comparing the load–displacement curves of a-C, a-C:NCG, and a-C:NCD films in Figs. 5–7, the differences of nanoindentation behaviors among the three kinds of films get greater and greater upon increasing nanoindentation load.

4. Discussion

In the present study, NCG clusters were embedded in the amorphous matrix, and the basal planes of NCG were cross-linked with each other by waving and twisting, as shown in Fig. 1(b)–(e). The bond between the graphitic basal planes is weak van der Waals' force. However, in the NCG cluster, the sp^2 bond between the neighbor atoms in a basal plane can be broken by ion irradiation, producing the unstable and swaying dangling bonds. If two dangling bonds encountered or the dangling bond links with the neighbor atom, a new sp^2 or sp^3 bond is generated to cross link the basal planes. Comparing with the a-C film, the percentage of elastic recovery increased for the a-C:NCG film, this is presumably because the cross links formed between the graphitic basal planes strengthened the resistance of basal planes to the tensile and compress strains, resulting in a more elastic structure [34]. While for the a-C:NCD film, the sp^3 content increased forming the nanocrystalline diamond clusters, both the elasticity and the hardness decreased. The reason for lower elastic recovery is considered to be the lower flexibility of sp^3 bond in NCD clusters. Although the hardness increases with the increasing of sp^3 bond content in amorphous carbon film, we measured a contrary result that the hardness of a-C:NCD film is lower than those of a-C and a-C:NCG films, which is supposed that when the grain size of NCD clusters is small, and the grain boundary sliding becomes more active in micro-deformation process, referred to as the "reverse Hall–Petch effect" [35]. Hence, the embedded NCD clusters weakened the overall mechanical property analyzed in the nanoindentation.

When the indentation load increased, the loading curves of a-C:NCG and a-C:NCD films show pop-in steps, as shown in Figs. 6 and 7. It should be mentioned that although the films showed a much rougher surface than a-C film, the domes were distributed dispersedly, height scan was performed to move the asperities away from the indentation center before the test, and a flat area was chosen to avoid the effects of surface roughness on the appearance of pop-ins during indentation. Moreover, no pop-out appeared neither in the unloading curves of carbon films nor in that of Si substrate, which means that no press induced phase transformation happened in the substrate [36]. Thereafter, pop-in steps occurred in the film independent of the surface roughness and the steps are not induced by the silicon substrate.

Then, the effect of carbon films on the appearance of pop-in steps is considered. It has been revealed that these steps are also related to the dislocations in the film structure [24] or brittle fracture through the film thickness [37]. For the pop-ins with about 3 nm displacements, the steps are much smaller than the film thickness and the steps only existed in the films with nanocrystalline clusters, it is inferred that the pop-in steps are caused by the dislocations in the structure of films containing NCG or NCD clusters. For the a-C:NCG and a-C:NCD films, nanocrystalline clusters embed in the amorphous matrix forming the local discontinuities in the structure, and dislocations exist in the film. During indentation, the first appearance of pop-in indicates the onset of dislocation plasticity when the maximum shear stress under the indenter is high enough [38], and the critical shear stress for heterogeneous is much smaller than that of homogeneous [39]. Therefore, upon increasing the indentation load, pop-ins appeared in the a-C:NCG and a-C:NCD films other than in the a-C film. Meanwhile, the motion of preexisting dislocations, the size, the density and the strength of

defects (NCG and NCD clusters) also affect the appearance of pop-in [24], these complicated factors result in the stochastic behavior of pop-ins with different indentation loads. As the maximum indentation load became greater, a large step appeared for the a-C:NCD film at the maximum indentation load, the sudden increase in displacement happened at an indentation depth deeper than the film thickness, which means that after the indenter has penetrated to the substrate, a through thickness crack can be generated for the brittle diamond clusters embedded film, resulting in a separation of partial film under or around the indenter from the film. Then, the stresses which partly support the indenter are suddenly removed to form a large discontinuity. The nanoindentation behaviors of a-C:NCG and a-C:NCD films were obtained with small load, and it is difficult to find the small impressions by the small observation area of AFM or SEM. In order to clarify the mechanism of nanoindentation behavior, the deformation processes of a-C:NCG and a-C:NCD films during nanoindentation will be observed by *in situ* TEM in the near future.

5. Conclusions

Nanostructures in a-C films were controlled by RF sputtering. NCG clusters occurred in the purely amorphous structure and the size and content increased with the increasing of ion energy to 120 eV and deposition temperature to 370 K. Both NCG and NCD clusters formed in the amorphous matrix when the film was deposited with ion energy of 120 eV and temperature of 570 K. The a-C:NCG films with cross-linked graphitic basal planes showed higher elastic recovery than that of pure a-C film, while, a-C:NCD films showed a lower elastic recovery. Comparing with the continuous loading curve of pure a-C film, pop-in steps occurred both in the loading curves of a-C:NCG and a-C:NCD films, and the a-C:NCD film showed a much larger pop-in step than the a-C:NCG film. The results showed that the nanoindentation behaviors of amorphous carbon films containing nanocrystalline graphite clusters are better than that of diamond clusters. This study indicates that the dependence of nanoindentation behavior on cluster characteristics should be considered in application.

Acknowledgements

The main author is very grateful to Associate Professor Makoto Kambara of the University of Tokyo for his help in arranging experimental equipment. This work is partially supported by the National Nature Science Foundation of China (Grant Number: 90923027), the China Postdoctoral Science Foundation (Grant Number: 2012M521755), and the PhD Mobility Program of the China Scholarship Council.

References

- [1] P.K. Chu, L.H. Li, Characterization of amorphous and nanocrystalline carbon films, *Materials Chemistry and Physics* 96 (2006) 253–277.
- [2] R.G. Lacerda, P. Hammer, C.M. Lepienski, F. Alvarez, F.C. Marques, Hard graphitic-like amorphous carbon films with high stress and local microscopic density, *Journal of Vacuum Science and Technology A* 19 (2001) 971–975.
- [3] Q. Wang, C.B. Wang, Z. Wang, J.Y. Zhang, D.Y. He, Fullerene nanostructure-induced excellent mechanical properties in hydrogenated amorphous carbon, *Applied Physics Letters* 91 (2007) 141902.
- [4] V.L. Kuznetsov, Y.V. Butenko, A.L. Chuvilin, A.I. Romanenko, A.V. Okotrub, Electrical resistivity of graphitized ultra-disperse diamond and onion-like carbon, *Chemical Physics Letters* 336 (2001) 397–404.
- [5] S. Hirono, S. Umamura, M. Tomita, R. Kaneko, Super-hard conductive carbon nano-crystallite films, *Applied Physics Letters* 80 (2002) 425–427.
- [6] Y.J. Wang, H.X. Li, L. Ji, F. Zhao, Q.H. Kong, Y.X. Wang, X.H. Liu, W.L. Quan, H.D. Zhou, J.M. Chen, Microstructure, mechanical and tribological properties of graphite-like amorphous carbon films prepared by unbalanced magnetron sputtering, *Surface and Coatings Technology* 205 (2011) 3058–3065.
- [7] P. Hojati-Talemi, G.P. Simon, Enhancement of field emission of carbon nanotubes using a simple microwave plasma method, *Carbon* 49 (2011) 484–486.
- [8] C. Wang, D.F. Diao, X. Fan, C. Chen, Graphene sheets embedded carbon film prepared by electron irradiation in ECR plasma, *Applied Physics Letters* 100 (2012) 231909.
- [9] D.W.M. Lau, D.G. McCulloch, M.B. Taylor, J.G. Partridge, D.R. McKenzie, N.A. Marks, E.H.T. Teo, B.K. Tay, Abrupt stress induced transformation in amorphous carbon films with a highly conductive transition phase, *Physical Review Letters* 100 (2008) 176101.
- [10] E.H.T. Teo, J. Kulik, Y. Kauffmann, R. Kalish, Y. Lifshitz, Nanostructured carbon films with oriented graphitic planes, *Applied Physics Letters* 98 (2011) 123104.
- [11] E. Cappelli, S. Orlando, G. Mattei, P. Zoffoli, Ascarelli SEM and Raman investigation of RF plasma assisted pulsed laser deposited carbon films, *Applied Surface Science* 197–198 (2002) 452–457.
- [12] J. Eskusson, R. Jaanisoo, E. Lust, Diamond-like phase formation in an amorphous carbon films prepared by periodic pulsed laser deposition and laser irradiation method, *Applied Surface Science* 255 (2009) 7104–7108.
- [13] J. Schwan, S. Ulrich, T. Theel, H. Roth, H. Ehrhardt, P. Becker, S.R.P. Silva, Stress-induced formation of high-density amorphous carbon thin films, *Journal of Applied Physics* 82 (1997) 6024–6030.
- [14] S. Logothetidis, M. Gioti, P. Patsalas, C. Charitidis, Insights on the deposition mechanism of sputtered amorphous carbon films, *Carbon* 37 (1999) 765–769.
- [15] K. Nose, K. Tachibana, T. Yoshida, Rectification properties of layered boron nitride films on silicon, *Applied Physics Letters* 83 (2003) 943–945.
- [16] D. Wan, K. Komvopoulos, Transmission electron microscopy and electron energy loss spectroscopy analysis of ultrathin amorphous carbon films, *Journal of Materials Research* 19 (2004) 2131–2136.
- [17] D. Wan, K. Komvopoulos, Formation of diamondlike nanocrystallites in amorphous carbon films synthesized by radio-frequency sputtering, *Journal of Materials Research* 23 (2008) 700–703.
- [18] D.W.M. Lau, A. Moafi, M.B. Taylor, J.G. Partridge, D.G. McCulloch, R.C. Powles, D.R. McKenzie, The structural phases of non-crystalline carbon prepared by physical vapor deposition, *Carbon* 47 (2009) 3263–3270.
- [19] C. Iwamoto, H.S. Yang, S. Watanabe, T. Yoshida, Dynamic and atomistic deformation of sp^2 -bonded boron nitride nanoarrays, *Applied Physics Letters* 83 (2003) 4402–4404.
- [20] J. Neidhardt, Z. Czigany, L. Hultman, Superelastic fullerene-like carbon nitride coatings synthesized by reactive unbalanced magnetron sputtering, *Surface Engineering* 19 (2003) 299–303.
- [21] Z. Wang, J.Y. Zhang, Deposition of hard elastic hydrogenated fullerene-like carbon films, *Journal of Applied Physics* 109 (2011) 103303.
- [22] W. Guo, C.Z. Zhu, T.X. Yu, C.H. Woo, B. Zhang, Y.T. Dai, Formation of sp^3 bonding in nanoindented carbon nanotubes and graphite, *Physical Review Letters* 93 (2004) 245502.
- [23] D.U. Michael, M.D. Dennis, N.F. Jeffrey, D.N. William, Sample dimensions influence strength and crystal plasticity, *Science* 305 (2004) 986–989.
- [24] J.R. Morris, H. Bei, G.M. Pharr, E.P. George, Size effects and stochastic behavior of nanoindentation pop in, *Physical Review Letters* 106 (2011) 165502.
- [25] O. Tsuda, Y. Yamada, T. Fujii, T. Yoshida, Preparation of cubic boron nitride films by radio frequency bias sputtering, *Journal of Vacuum Science and Technology A* 13 (1995) 2843–2847.
- [26] O. Tsuda, Y. Tatebayashi, Y. Takamura-Yamada, T. Yoshida, Mass and energy measurements of the species responsible for cBN growth in rf bias sputter conditions, *Journal of Vacuum Science and Technology A* 15 (1997) 2859–2863.
- [27] H. Sjöström, L. Hultman, J.E. Sundgren, S.V. Hainsworth, T.F. Page, G.S.A.M. Theunissen, Structural and mechanical properties of carbon nitride CN_x ($0.2 \leq x \leq 0.35$) films, *Journal of Vacuum Science and Technology A* 14 (1996) 56–62.
- [28] M. Chhowalla, A.C. Ferrari, J. Robertson, G.A.J. Amaratunga, Evolution of sp^2 bonding with deposition temperature in tetrahedral amorphous carbon studied by Raman spectroscopy, *Applied Physics Letters* 76 (2000) 1419–1421.
- [29] A.C. Ferrari, J. Robertson, Resonant Raman spectroscopy of disordered, amorphous, a diamondlike carbon, *Physical Review B* 64 (2001) 075414.
- [30] J.O. Orwa, I. Andrienko, J.L. Peng, S. Praver, Y.B. Zhang, S.P. Lau, Thermally induced sp^2 clustering in tetrahedral amorphous carbon (ta-C) films, *Journal of Applied Physics* 96 (2004) 6286–6297.
- [31] A.C. Ferrari, S.E. Rodil, J. Robertson, W.I. Milne, Is stress necessary to stabilize sp^3 bonding in diamond-like carbon? *Diamond and Related Materials* 11 (2002) 994–999.
- [32] W.C. Oliver, G.M. Pharr, An improved technique for determining hardness and elastic modulus using load and displacement sensing indentation experiments, *Journal of Materials Research* 7 (1992) 1564–1583.
- [33] T.F. Page, S.V. Hainsworth, Using nanoindentation techniques for the characterization of coated systems: a critique, *Surface and Coatings Technology* 61 (1993) 201–208.
- [34] M.K. Zalalutdinov, J.T. Robinson, C.E. Junkermeier, J.C. Culbertson, T.L. Reinecke, R. Stine, P.E. Sheehan, B.H. Houston, E.S. Snow, Engineering graphene mechanical systems, *Nano Letters* 12 (2012) 4212–4218.
- [35] I.N. Remediakis, G. Kopidakis, P.C. Kelires, Reverse Hall–Petch effect in ultra nanocrystalline diamond, in: *Proceedings of the IUTAM Symposium on Modelling Nanomaterials and Nanosystems*, Aalborg, Denmark, May 19–22, 2008.

- [36] T. Juliano, V. Domnich, Y. Gogotsi, Examining pressure-induced phase transformations in silicon by spherical indentation and Raman spectroscopy: a statistical study, *Journal of Materials Research* 19 (2004) 3099–3108.
- [37] X.D. Li, D.F. Diao, B. Bhushan, Fracture mechanisms of thin amorphous carbon films in nanoindentation, *Acta Materialia* 45 (1997) 4453–4461.
- [38] S. Shim, H. Bei, E.P. George, G.M. Pharr, A different type of indentation size effect, *Scripta Materialia* 59 (2008) 1095–1098.
- [39] H. Bei, Y.F. Gao, S. Shim, E.P. George, G.M. Pharr, Strength differences arising from homogeneous versus heterogeneous dislocation nucleation, *Physical Review B* 77 (2008), 060103.